npj | climate and atmospheric science

Article

Published in partnership with CECCR at King Abdulaziz University

https://doi.org/10.1038/s41612-024-00726-x

Enhanced formation of nitrogenous organic aerosols and brown carbon after aging in the planetary boundary layer

Yangzhou Wu[1,2], Quan Liu[3], Dantong Liu[2] ✉, Ping Tian[4], Weiqi Xu[5], Junfeng Wang[6], Kang Hu[2,6], Siyuan Li[2], Xiaotong Jiang[2,7], Fei Wang[4], Mengyu Huang[4], Deping Ding[4], Chenjie Yu[8] & Dawei Hu[9]

Particulate organic nitrates (pON) significantly contribute to the mass of organic aerosol and influence the nitrogen oxides cycle in the atmosphere, but their evolution and lifetime remain uncertain. This study performed simultaneous measurements on the anthropogenically affected surface site and the mountain site on top of the polluted planetary boundary layer (PBL). After aging in the PBL, organic nitrate was converted from primary sources (decreased from 8.7% to 4.3%) to secondary sources (increased from 6.3% to 36.1%), spanning from the surface to the mountain. The evaporation of more volatile inorganic nitrate and the production of secondary organic nitrate during aging in the PBL contributed to the enhanced pON fraction over the top of PBL. The contribution of light absorption by brown carbon increased by 57% at the top of PBL compared to the surface, consistent with the higher fraction of nitrogenous organic aerosols over the mountain. The results provide field evidence that the nitrogenous organic aerosols (OA) may be preserved by adding into secondary OA and significantly contribute to the enhanced importance of brown carbon after aging during vertical transport in the PBL.

In recent years, anthropogenic activities such as the excessive application of fertilizers[1], fossil fuel combustion[2], and industrial processes[3] have disrupted the natural nitrogen cycle, leading to increased levels of reactive nitrogen species in the environment. Furthermore, nitrogen imbalances exacerbate climate change-related impacts, including biodiversity shifts[4] and altered ecosystem functions[5]. Particulate organic nitrates (pON) form in the atmosphere through the oxidation of volatile organic compounds (VOCs) in the presence of nitrogen oxide family radicals and can contribute to the formation of secondary organic aerosols[6]. pON has been shown to contribute a substantial mass (5 - 77%) to organic aerosol (OA)[7], and it can offer a reservoir of nitrogen oxides (NO_X) and may be associated with ozone (O_3) production[8–10]. The filter analysis is widely used to quantify the molecular compositions of pON using gas chromatography[11] or Fourier transformed infrared[12]. In online measurement techniques, the thermal dissociation method is used to derive organic nitrates by dissociating the pON into NO_2 and subtracting from the background NO_2, characterized by laser-induced fluorescence (LIF), cavity ring-down spectroscopy, or cavity-attenuated phase shift spectroscopy[13–15].

The high-resolution time-of-flight aerosol mass spectrometer (HR-ToF-AMS) can provide online characterization of fragments. The main principle of the "NOx^+ method" is that the NO_2^+/NO^+ ratio of pON is different from that of inorganic nitrate[16–18]. The positive matrix factorization (PMF) method was also used to quantify pON, referred to as "PMF method". The fragments of NOx^+ are also added to the mass spectrum of OA for the PMF analysis[19–21]. Given that AMS can measure not only nitrate fragments but also other ON-associated fragments like $C_xH_yO_zN^+$, these fragments can be used as markers for pON. A thermodenuder was used to measure supposed pON residuals above 90 °C, and nitrogenous fragments were utilized to calculate the fraction of ON remaining at high temperatures[22].

[1]Guangxi Key Laboratory of Theory and Technology for Environmental Pollution Control, Collaborative Innovation Center for Water Pollution Control and Water Safety in Karst Area, Guilin University of Technology, Guilin, China. [2]Department of Atmospheric Sciences, School of Earth Sciences, Zhejiang University, Hangzhou, China. [3]State Key Laboratory of Severe Weather & Key Laboratory of Atmospheric Chemistry of CMA, Chinese Academy of Meteorological Sciences, Beijing, China. [4]Beijing Weather Modification Center, Beijing, China. [5]State Key Laboratory of Atmospheric Boundary Layer Physics and Atmospheric Chemistry, Institute of Atmospheric Physics, Chinese Academy of Sciences, Beijing, China. [6]Jiangsu Key Laboratory of Atmospheric Environment Monitoring and Pollution Control, Collaborative Innovation Center of Atmospheric Environment and Equipment Technology, Joint International Research Laboratory of Climate and Environment Change, School of Environmental Science and Engineering, Nanjing University of Information Science and Technology, Nanjing, China. [7]College of Biological and Environmental Engineering, Shandong University of Aeronautics, Binzhou, China. [8]Université Paris Cité and Univ Paris Est Créteil, CNRS, LISA, Paris, France. [9]Department of Earth and Environmental Sciences, University of Manchester, Manchester, UK. ✉e-mail: dantongliu@zju.edu.cn

The main pathway for the formation of secondary pON is through the oxidation of gas precursors, which can be either biogenic (commonly isoprene) or anthropogenic (commonly alkanes), during daytime by hydroxyl radicals (HO·) followed by the addition of O_2 and NO[23–25] or during nighttime by NO_3 radical oxidation[26]. A variety of primary emissions from combustion can also contribute to considerable pON[27,28]. The primary OA can undergo evolution, as indicated by both measurements[29] and model analysis[30]. Nitrogenous OA importantly contributes to light absorption as brown carbon (BrC)[31,32].

Most previous measurements were conducted at ground level, which had continuous influences from ground sources. In this study, we present simultaneous measurements of aerosol chemical composition and light absorption of aerosol particles at both surface and mountain sites influenced by the surface in Beijing, China. This offers an opportunity to study the evolution of pON in the planetary boundary layer (PBL). Sources of pON, determined using PMF analysis, were correlated with BrC light absorption to identify the major contributor to short-wavelength light absorption. More detailed chemical characteristics, such as pON mass concentration and nitrogenous ion fragments, were used to investigate the properties of BrC related to light absorption. By comparing the differences in sources of nitrogenous organic aerosol between the two sites, we aim to investigate the modification in light absorption during the upward transport in the PBL and explore the correlations between the absorption coefficient of BrC and pON.

Results and discussions

Mass concentrations and chemical composition at the mountain and surface

The real-time simultaneous measurements of aerosol particle composition at both the surface and mountain sites influenced by it are depicted in Supplementary Fig. 1. During the regional advection period, which originated from westerly winds (Supplementary Fig. 2), a significantly higher concentration of aerosols was observed at the mountain site due to the transport of regional pollutants from the polluted high plateau. The data only during the convective mixing period is used for the analysis in order to investigate the evolution of aerosols during vertical transport from the surface to the top of PBL, minimizing the influence of regional horizontal transport.

PM_1 mass concentration at the mountain was 2.7 ± 1.9 μg m^{-3}, which is 4.3 times lower than the surface value of 14.3 ± 7.1 μg m^{-3}. The average bulk aerosol composition was substantially different at the two heights. While organics dominated the total PM_1 mass at both the mountain and surface, accounting for 41% and 60%, respectively, the average mass concentration of organics at the mountain (1.5 μg m^{-3}) was significantly lower than that at the surface (11.5 μg m^{-3}). The higher concentration and contribution of organics observed at the surface were mainly attributed to the correspondingly higher primary organic matter from local sources (as discussed in the following section). Sulfate and nitrate showed equivalent contributions (11 vs 12%) to PM_1 at the surface, while sulfate was significantly higher than nitrate (28% vs 10%) in the mountain site.

The NO^+/NO_2^+ ratios (hereafter "RoR") at the mountain were remarkably higher than those at the surface (Supplementary Fig. 1), especially when the RH at the mountain is higher than that at the surface (Supplementary Fig. 2). A possible explanation is that the gas–particle partitioning of organic nitrate was facilitated at greater heights because of the lower T and higher RH compared to ground. Supplementary Fig. 1d shows the fraction ($f_{NO3,org}$) of total non-refractory submicron nitrate that is $NO_{3,org}$ vs. total nitrate mass loading (pNO_3) estimated using two different methods during the campaign. The $f_{NO3,org}$ calculated by the RoR method has a weaker correlation with those of the PMF method at the mountain ($r = 0.74$) and at the surface ($r = 0.67$). The differences between the two methods may be due to the PMF method's incorrect assignment of NO^+ and NO_2^+ to primary OA (POA) factors (Fig. 1) and that organic ions would be assigned to nitrate inorganic aerosol factor, consistent with previous studies[22]. However, the RoR method only estimates the bulk organic nitrate, and it is unable to separate primary and secondary sources further. Both methods have their advantages, so the results of both methods will be used in the following analysis, and the method used will be indicated.

Supplementary Figure 4 gives the statistical diurnal variations in aerosol species during the convective mixing period. The BC concentration on the mountain at midday to early afternoon almost matched that on the ground, indicating a well-mixed layer because of the daytime convective mixing (Supplementary Fig. 4b). The diurnal cycle of organics (Supplementary Fig. 4f) was similar to that of POA (Supplementary Fig. 4g) at the surface, with both factors showed two pronounced peaks. However, at the mountain site, their diurnal variations were relatively smoother. The potential explanation for the observed discrepancy lies in the elevated local emissions during morning and evening hours, encompassing traffic, cooking activities, and coal combustion. Additionally, the shallower boundary layer leads to reduced vertical mixing. Previous studies have indicated that POA contains a significant amount of semi-volatile materials and exhibits relatively high volatility[33]. The secondary OA (SOA), less-volatile organic aerosol, showed a clear diurnal pattern on the mountain, with concentrations elevated in the early afternoon. On the ground level, the diurnal variation in SOA concentration showed a minimum during the daytime due to the dilution effect of developed PBL. This result suggests that a significant portion of the SOA was mixed the mountain during the daytime. The aforementioned results demonstrate that, during vertical transport, particulate mass loss only occurs for semi-volatile substances (such as POA) rather than low-volatile species (like BC and SOA).

Enhanced fraction of nitrogenous organic aerosols after aging in the PBL

The mean differences of mass spectra for all OA fragments and specifically for all nitrogenous fragments between surface and mountain sites are shown in Fig. 1. The surface site showed a clearly enhanced contribution for almost all hydrocarbon fragments than the mountain (Fig. 1a). The mountain had a significantly higher fraction for the typical oxygen-containing fragment, such as m/z 29 (mainly CHO^+) and 44 (mainly CO_2^+), but a lower fraction of hydrocarbon fragments ($C_xH_{2x-1}^+$). The fresh OA emissions rich in hydrocarbons had been considerably aged during a few hours of vertical transport. This implies that the OA on the mountain is more aged and oxygenated, and its oxidation may occur at unsaturated bonds (e.g., alkenes)[34]. Figure 1b shows the fraction of all species of nitrogenous fragments that were enhanced on the mountain by 7%. This clearly demonstrates the higher oxidation state and nitrogen content for the aerosols on the mountain after vertical transport from surface sources.

The NO^+ and NO_2^+ signals detected by AMS can originate from the fragmentation of both particulate organic nitrate ($NO_{3,org}$) and inorganic nitrates (NH_4NO_3), whereas the nitrogenous organic fragments, mainly composed of CHN^+ and $CHON^+$, are exclusively derived from pON or other nitrogenous organic compounds. Figure 1c, d shows the concentration of $CHON^+$ correlated well with NO^+ ($r = 0.99$) and NO_2^+ ($r = 0.99$) at the mountain, but this correlation was rather weak at the ground ($r = 0.65$ and $r = 0.65$, respectively). It provides strong evidence that NO^+ and NO_2^+ fragments were more likely to exclusively result from nitrogenous OA on the mountain, whereas the surface NOx^+ fragments were largely contaminated by inorganic nitrate. This, in turn, implied that there was a more important fraction of nitrogenous OA on the mountain than on the surface. The reduced fraction of inorganic nitrate, which has been reduced, is consistent with our previous study, which found that ammonium nitrate evaporated during vertical transport due to its higher volatility[35].

Further attribution between organic and inorganic nitrate using PMF and RoR method showed enhanced $NO_{3,org}$ fraction within total nitrate with deceased total nitrate concentration (Fig. 1e), with mountain having a lower total pNO_3 and higher $NO_{3,org}/pNO_3$ fraction. The $f_{NO3,org}$ shows an inverse relationship with the pNO_3, approaching 100% at low pNO_3. The contribution of $NO_{3,org}$ exceeded 40% when pNO_3 was lower than < 1 μg m^{-3}. $f_{NO3,org}$ from the PMF method was lower than the RoR method at higher pNO_3 because of the larger contamination from inorganic nitrate but showed high consistency when pNO3 was lower than 1 μg m^{-3}.

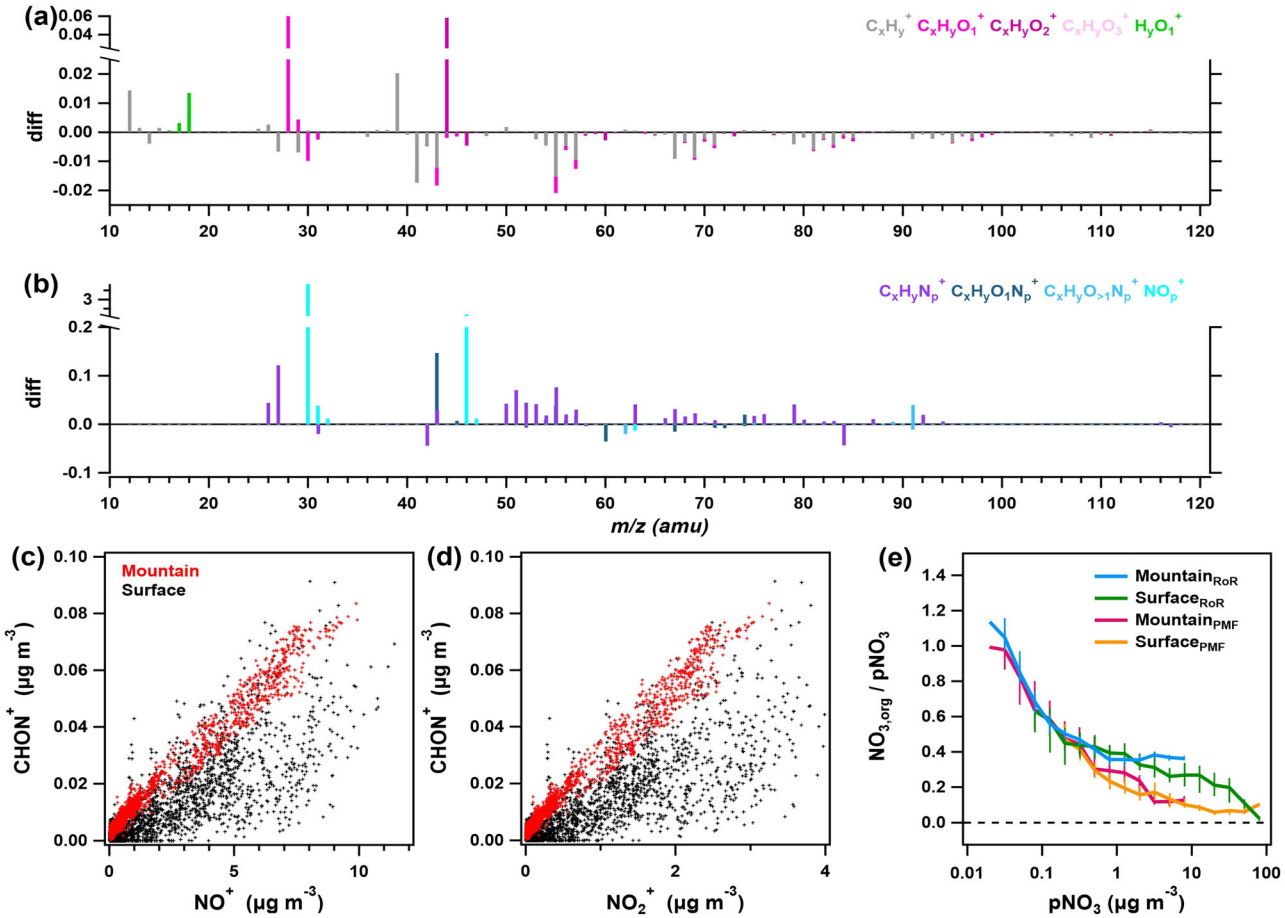

Fig. 1 | Organic aerosol variations and nitrogen-containing ions at mountain and surface sites, with correlations between $CHON^+$ and NO^+/NO_2^+. Difference in OA mass spectra between the mountain and surface sites (mountain minus surface) for (**a**) OA, and (**b**) all nitrogen-containing fragment ions. Scatterplot of (**c**) $CHON^+$ versus NO^+, and (**d**) $CHON^+$ versus NO_2^+. **e** Fraction of total non-refractory submicron nitrate that is organic ($NO_{3,org}/pNO_3$) versus total nitrate concentration (pNO_3) for mountain and surface site calculated using RoR method and PMF method. The Mountain and surface site using the RoR method are representes by $Mountain_{RoR}$ and $Surface_{RoR}$. The Mountain and surface site using the PMF method are representes by $Mountain_{PMF}$ and $Surface_{PMF}$.

Enhanced secondary particulate organic nitrate after aging in the PBL

The mass spectra for the PMF-resolved factors for the mountain and surface sites are shown in Fig. 2, and each factor is given a fraction of NO^+ and NO_2^+ fragments (f_{NOx}). In order to mitigate the influence of NO^+ and NO_2^+ fragments and facilitate comparison with previous studies, the N: C calculation in the figure excludes NO^+ and NO_2^+ fragments. The five factors identified for the mountain site include two primary factors, two oxygenated OA (OOA) factors, and a factor that is primarily inorganic nitrate ($NO_{3,inorg}$). Six factors are identified for the surface site. On both sites, the $NO_{3,inorg}$ with the highest f_{NOx} (about 60%), is mainly composed of inorganic nitrate, which has the NO^+/NO_2^+ ratios (2.7 for the surface, 2.8 for the mountain), close to the value (2.7) determined in pure ammonium nitrate.

The primary OA factors, hydrocarbon-like OA (HOA) and coal combustion OA (CCOA), were identified for both sites. The HOA (O/C = 0.17, f_{NOx} = 1.2% for the mountain and O/C = 0.14, f_{NOx} = 9.7% for the surface) were characterized by higher contributions of aliphatic hydrocarbons, e.g., m/z 43 ($C_3H_7^+$), 55 ($C_4H_7^+$) and 57 ($C_4H_9^+$). Besides the common hydrocarbons, the CCOA (O/C = 0.19, f_{NOx} = 16.0% for the surface and O/C = 0.25, f_{NOx} = 1.3% for the mountain) also showed pronounced signals of fragment at m/z = 115 (mainly $C_9H_7^+$), typically for the fragments from polycyclic aromatic hydrocarbons (PAHs)[36], which was widely observed from heating activities in cold season in Beijing region[37,38]. The CCOA showed a higher f_{NOx} on the mountain than on the surface because the same source had experienced an aging process after vertical transport from the surface to the mountain. The surface site had a factor of cooking OA with mark fragments of $C_3H_3O^+$ (m/z 55; r = 0.84) and $C_6H_{10}O^+$ (m/z 98; r = 0.94), but not for the mountain site, due to the more localized feature of cooking emissions. Note that the COA factor is almost completely organic with low f_{NOx} (0.6%, Fig. 2). The low fraction of $NO_{3,org}$ in COA indicates that the cooking process may not be an essential source of organic nitrate. Previous studies have also found that f_{NOx} in COA was low when PMF analysis was performed on the combined organic and inorganic mass spectra[19,22,39].

Secondary oxygenated OA with two levels of oxidation states, the semi-volatile OA (SV-OOA) and lower-volatile OA (LV-OOA), were identified. The LV-OOA had a higher dominant peak of m/z 44 (mainly CO_2^+) and a highest O/C ratio (O/C = 0.76, f_{NOx} = 3.5% for the mountain and O/C = 0.64, f_{NOx} = 0.4% for the surface); while SV-OOA had a lower O/C (O/C = 0.48, f_{NOx} = 8.2% for the mountain and O/C = 0.44, f_{NOx} = 5.3% for the surface) with higher peaks at m/z 29 (mainly CHO^+) and 43 (mainly $C_2H_3O^+$).

The NO^+ and NO_2^+ had contrasting fractions in the mass spectra (f_{NOx}) between POA and SOA. On the surface, HOA and CCOA had the highest f_{NOx} at 9.7% and 16.0% respectively. This suggests the fossil fuel and coal combustion sources were rich in organic nitrate compounds. Previous studies observed high nitrogen content in OA from coal combustion[40,41]. Notably, the f_{NOx} fraction for POA dramatically dropped on the mountain by about 8.5% and 14.7% for HOA and CCOA, respectively. This is contrast for $NO_{3,org}$ in SOA, which is from surface to mountain, f_{NOx} in SV-OOA increased from 5.3% to 8.2% and increased from 0.4% to 3.5% for LV-OOA. The decreased $NO_{3,org}$ fraction in POA but increased fraction in SOA clearly

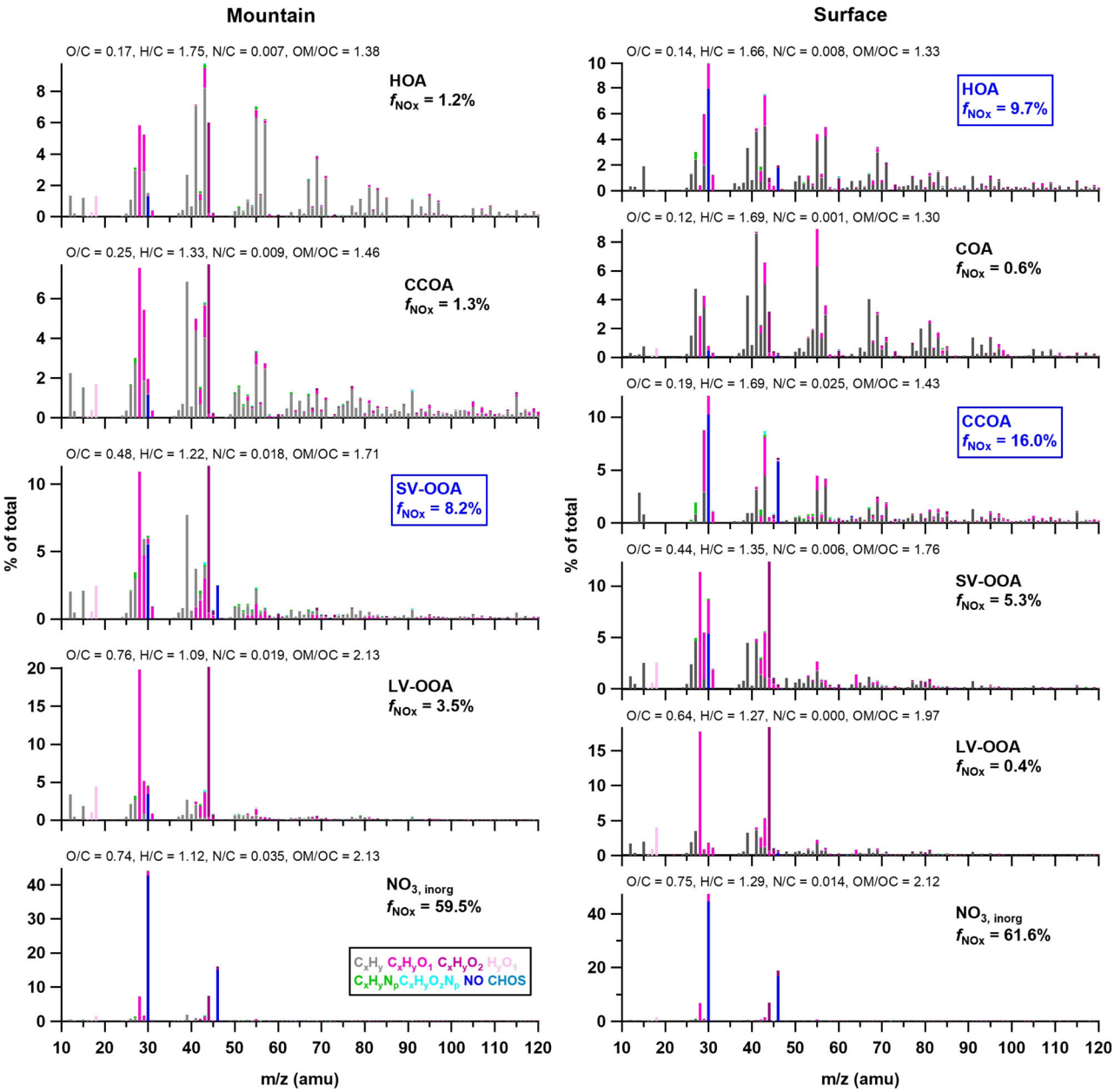

Fig. 2 | Mass spectra of organic factors derived from the data of the mountain and surface site. Five factors were resolved from the mountain OA, including hydrocarbon-like OA (HOA), coal combustion OA (CCOA), semi-volatile oxygenated OA (SV-OOA), low volatility oxygenated OA (LV-OOA), and primarily inorganic nitrate ($NO_{3,inorg}$). Six factors were identified from the surface OA, i.e., HOA, cooking OA (COA), CCOA, SV-OOA, LV-OOA, $NO_{3,inorg}$. The mean contribution of NO^+ plus NO_2^+ (f_{NOx}) is indicated for each factor. In order to mitigate the influence of NO^+ and NO_2^+ fragments and facilitate comparison with previous studies, the N: C calculation in the figure excludes NO^+ and NO_2^+ fragments.

indicated a conversion of $NO_{3,org}$ from POA to SOA during aging in the PBL. The reduced fraction of $NO_{3,org}$ in POA, contrasted with its increased fraction in SOA, clearly indicates that at the surface site, organic nitrate is predominantly associated with POA. However, during transport to the mountain, it is predominantly found within SOA.

Figure 3 shows the histograms for each fraction of source-attributed nitrate during the convective mixing period. The inorganic nitrate dominated the total nitrate at the mountain and surface sites, accounting for 60 ± 25% and 89 ± 15%, respectively (Fig. 3a, b). The lower concentration and contribution of NH_4NO_3 observed at the mountain were primarily caused by the correspondingly higher volatility of inorganic nitrates during vertical transport. For the nitrate in organic aerosol, the surface and mountain sites showed contrasting source attributions. Supplementary Fig. 2 showed clearly enhanced $NO_{3,org}$ in SOA on the mountain than the surface, with the most pronounced shift for the $NO_{3,org}$ in semi-volatile OA. The average contributions of $NO_{3,org}$ in HOA and CCOA at the surface (3.7 ± 5.0% and 3.7 ± 4.3%) were both higher than that at the mountain (1.6 ± 1.9% and 2.7 ± 3.0%) to the total nitrate. However, the contributions of $NO_{3,org}$ in SV-OOA and LV-OOA showed larger total nitrate at the mountain (19.8 ± 13.4% and 16.4 ± 18.9%), which are both higher than those at the surface (5.3 ± 7.2% and 1.0 ± 2.4%).

The narrow and right-shifted frequency distributions of inorganic nitrate reflect the typical trend that NH_4NO_3 tends to constitute higher fractions when the total pNO_3 is higher (Fig. 3c, d). The histogram analysis for $NO_{3,org}$ in SV-OOA presents a distinct peak frequency at nitrate mass fraction of ~ 30% at the mountain (Fig. 3c). $NO_{3,org}$ in LV-OOA showed higher and broad distribution on the mountain than the surface. The peaks at ~ 3-4% of $NO_{3,org}$ in CCOA and HOA were obtained at the surface site

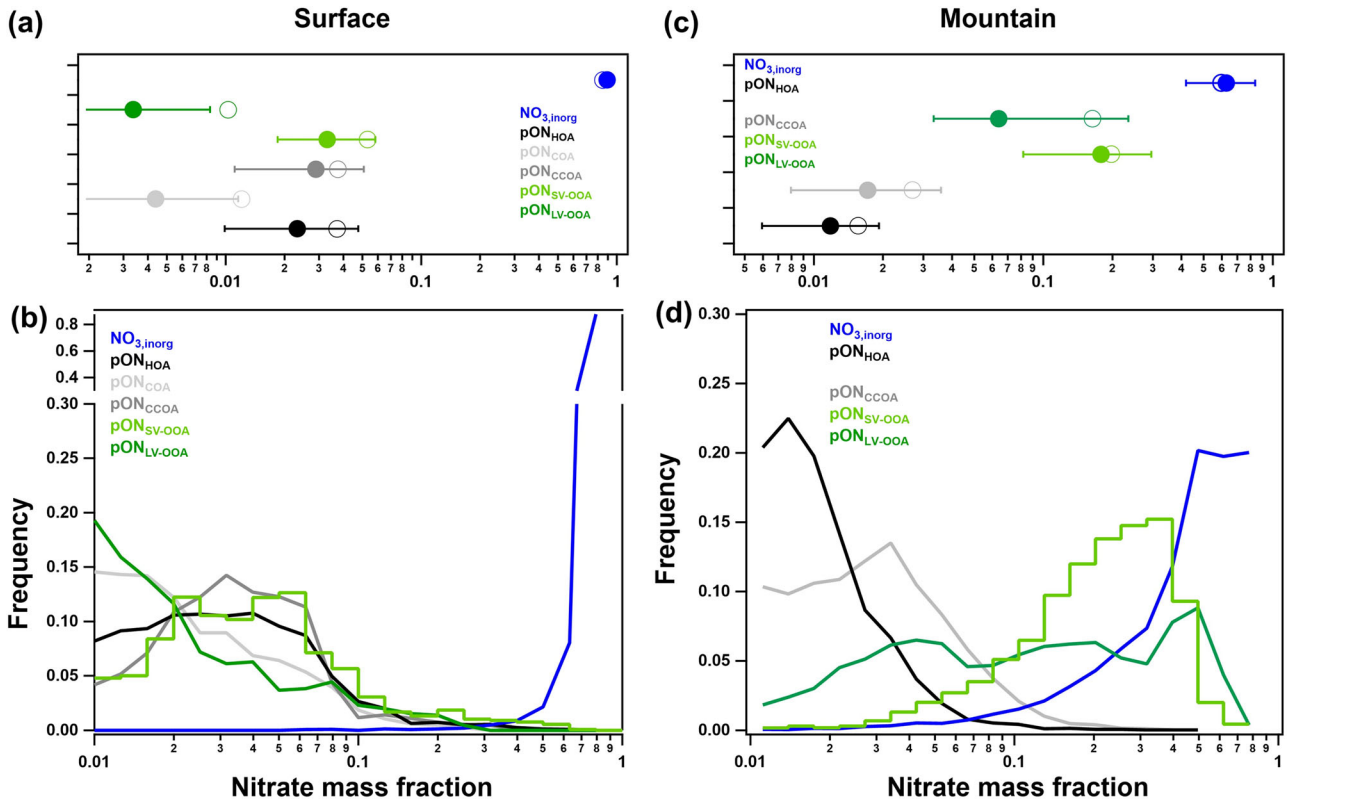

Fig. 3 | Histograms of PMF factors, inorganic nitrate, and organic nitrate in each factor with nitrate mass fraction for the surface and mountain site. a, **b** The circles and triangles indicate the median and mean values, the upper and lower boundaries indicate the 75th and 25th percentiles. **c**, **d** The distribution of inorganic nitrate and organic nitrate (presented as a normalized histogram) in each factor.

(Fig. 3d), which are significantly higher than the results at the mountain (~2% and ~3% for CCOA and HOA, respectively), whereas the nitrate fraction peaks were observed to be much lower for SV-OOA (~4–6%) and LV-OOA (<1%) at the surface.

At the mountain, the $NO_{3,org}$ was tightly correlated with SOA ($r = 0.92$) but weakly correlated with POA for most of the time ($r = 0.79$). These results indicate that $NO_{3,org}$ on the mountain was dominantly from secondary formation, consistent with the dominant contributions of SOA (69 ± 18%) to OA. The organic nitrate associated with SOA at the mountain exhibited a higher contribution to total nitrate compared to that at the surface. However, a higher concentration and contribution of $NO_{3,org}$ associated with POA were observed at the surface, indicating that the $NO_{3,org}$ at the mountain was mainly from secondary organic nitrate, while the surface was mainly primary organic nitrate. Here, by concurrently measuring close to the surface emission and over the top of the PBL influenced by the same surface emission, we clearly showed a conversion of $NO_{3,org}$ from POA to SOA.

Enhanced light absorption of brown carbon after vertical transport in the PBL

At the mountain, the diurnal profiles of primary sources and OA factors exhibited a consistent gradual increase from noon until late afternoon (Supplementary Figs. 4 and 5). This increase was due to the development of the PBL (Supplementary Fig. 4a) when the surface pollutants were transported upwards through convective mixing. The more pronounced diurnal peak of SV-OOA than other POA indicated the possible additional production of OA mass through photochemical processes, particularly during the upward transport. The surface showed considerably enhanced concentrations for all pollutions (Supplementary Fig. 6) due to the shallow PBL at night, though with different patterns for certain aerosol types.

The fraction of $NO_{3,org}$ in total nitrate was approximately 0.33, with low diurnal variation observed on the surface (Fig. 4a). The mountain showed a higher $NO_{3,org}$ fraction (59 ± 24%) than that at the surface (33 ± 15%) throughout the day. A decrease of $NO_{3,org}$ fraction on the mountain showed in the afternoon, which corresponded with the increase of inorganic nitrate when influenced mainly by the convective mixing of surface sources. Following the intrusion of surface pollutants, the elevated pON fraction implied a more likely rapid formation of pON compared to inorganic nitrate during the aging and dilution processes on the mountain. The even higher $NO_{3,org}$ fraction indicated the transported nitrates may undergo further aging and become incorporated into OA.

At the surface site, $NO_{3,org}$ in both POA and SOA typically showed diurnal patterns for urban environments following the development of PBL, which was diluted by the daytime-developed PBL but accumulated when shallow PBL. The mountain however showed contrasting diurnal patterns with no apparent diurnal variation for pON in POA, but pON in SOA showed substantially elevated concentration in the afternoon at the mountain (Fig. 4c), coincident with the peak of O_3 (Supplementary Fig. 4). This suggested that the enhancement of secondary pON on the mountain may be caused by photochemical production. This process tended to occur within a few hours from surface emission, and within this time, pON in primary emissions was converted into a secondary state. The reduced fraction of primary pON could be partly attributed to the photolysis of the primary pON[42]. The degradation of OA was evidenced by a reduced fraction of large molecular OA, on the mountain, the OA mass spectra with large m/z were significantly reduced compared to the surface (Fig. 1a). Photooxidation may have occurred in the gas phase and formed pON through the HO· oxidation of aromatics and NO_2 pathway[43]. The production of $NO_{3,org}$ via photooxidation may also be evidenced by the enhancement of N/C ratio on the surface (Fig. 4d). Figure 4d shows that the surface exhibited an elevated N/C ratio, possibly due to photochemical processes occurring in the early

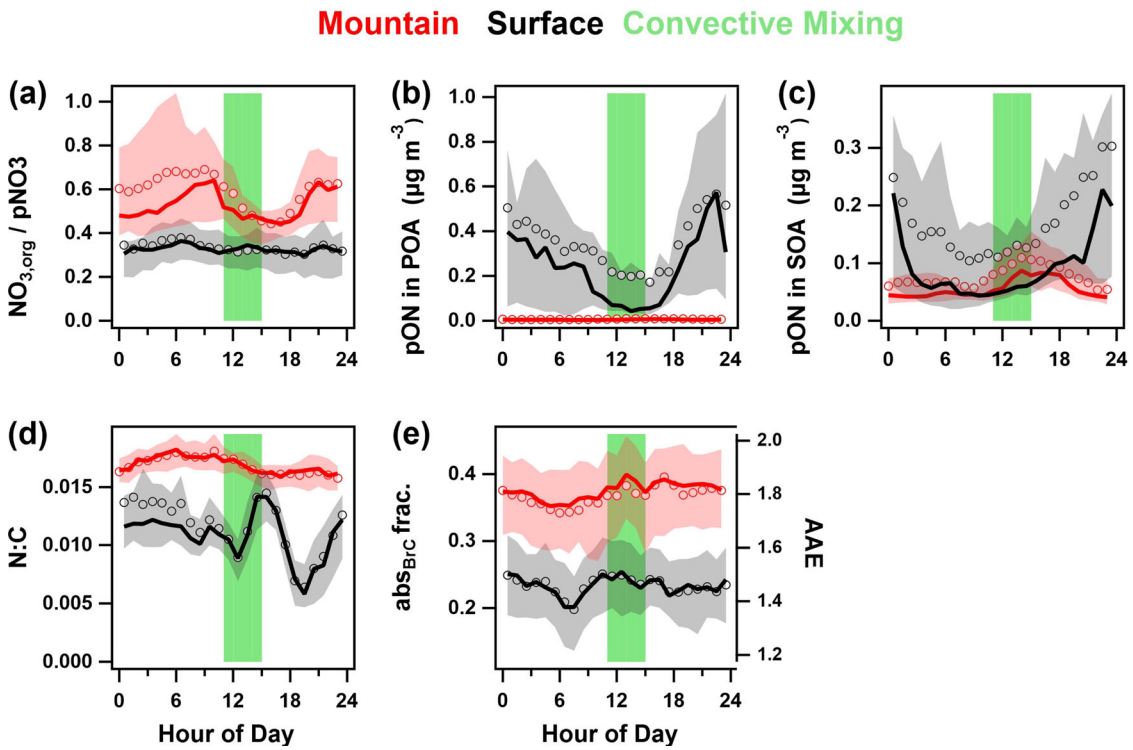

Fig. 4 | Diurnal profiles of various species at the mountain and surface sites. Diurnal profiles of (**a**) the fraction organic nitrate in total particulate nitrate ($NO_{3,org}/pNO_3$), mass concentrations of particulate organic nitrates in primary OA (**b**) and secondary OA (**c**), (**d**) nitrogen-to-carbon ratio (N:C), (**e**) absorbing Ångström exponent (AAE, right axis) and fraction of brown carbon (BrC) absorption in total absorption (abs_{BrC}) at λ = 370 nm (left axis). The green bar represents the time of the day (11:00–14:00) with the most developed PBL. The lines and circles represent the median and mean values, with the shaded upper and lower boundaries indicating the 75th and 25th percentiles, respectively.

afternoon, as also observed by previous studies[19,40]. The mountain site had a higher N/C at 0.017 ± 0.001 with minor variations throughout the day. The slight increases in N/C likely indicated an aging process since the midday injection of fresher surface sources.

Figure 4e shows that the absorption Ångström exponent (AAE) at the surface is lowest around 7:00 am, which may be caused by the fresher sources containing a higher fraction of BC during the morning rush hour. Importantly, it showed remarkably enhanced the AAE at the mountain (1.81 ± 0.04) than that at the surface (1.46 ± 0.03), corresponding with a high BrC contribution from 23.3 ± 1% to 36.7 ± 1% (Fig. 4e). The higher BrC contribution on the mountain throughout the day had not been affected by fresher sources from surface. These results indicated that the enhanced BrC contribution could occur within a few hours of upward transport in the PBL.

Figure 5 summarizes the factors that may account for the enhanced BrC contribution. During the convective mixing period, from the surface to the mountain, the nitrate fraction in total nitrate increased from 0.33 ± 0.12 to 0.51 ± 0.25, with O/C and N/C increasing from 0.41 ± 0.09 to 0.61 ± 0.06, and from 0.02 ± 0.004 to 0.03 ± 0.002, respectively. The nitrogenous OA-related fragments, specifically f_{CHN}^{+} and f_{CHON}^{+}, increased from 0.41 ± 0.09 to 0.61 ± 0.06 and from 0.02 ± 0.004 to 0.03 ± 0.002, respectively. These all indicate the more important contribution of nitrogenous OA to total OA over the top of PBL after aging in the PBL. Both O/C and N/C ratios increased by 0.5 and 0.5, respectively (Fig. 5 and Supplementary Fig. 9), implying that the aging of OA may involve the chemical reactions adding oxygen and nitrogen. As indicated in Supplementary Fig. 9, N/C increased almost linearly as O/C increased, suggesting the formation of more nitrogenous compounds during the aging of OA from the surface to the mountain. The organic nitrate and other nitrogenous OA will be produced in a secondary state after transport in the PBL. These secondary formations of pON may involve the production of nitroaromatics by adding NO_2 to anthropogenic aromatics[44], or organic nitrate formation by the NO_3 oxidation of VOCs[20,45] or HO· initiated gas-phase reactions with NO_X[43], all of which will simultaneously increase the N/C and O/C after aging. AAE increased by 24.0 ± 3.9%, corresponding with an increased BrC fraction of 57.3 ± 1.3% from surface to mountain. The continuous injection of pollutants from the surface emissions during the daytime convective mixing period, and further aging at night in the residue layer[46] will maintain the consistently high nitrogenous OA content and the corresponding AAE. Supplementary Figure 11 shows that there is a close relationship between brown carbon absorption and nitrogenous OA, and the mountain site had a higher pON fraction and AAE than the surface site. This means the brown carbon may persist after aging, extending its lifetime and radiative and health impacts.

Here by concurrent measurement close to the surface emission and over the top of PBL influenced by the same surface emission in regional scale, we found a higher fraction of organic nitrate and other nitrogenous organic aerosols (OA) on the mountain than on the surface. A conversion of particulate organic nitrate from being dominant from primary to secondary OA when pollutants were transported upwards in the boundary layer. The light absorption of aerosols at shorter wavelength was found to be more pronounced at higher altitudes, indicating a greater presence of atmospheric brown carbon in the upper boundary layer compared to the surface. This observation aligns with the elevated nitrogenous organic compounds detected in the mountain region. These findings imply that the enhanced presence of nitrate contained in organic aerosols, particularly in remote places after aging. Along with the other nitrogenous OA, these aerosols may have a longer lifetime, extending their impacts on nitrogen cycle and radiative impacts in the atmosphere.

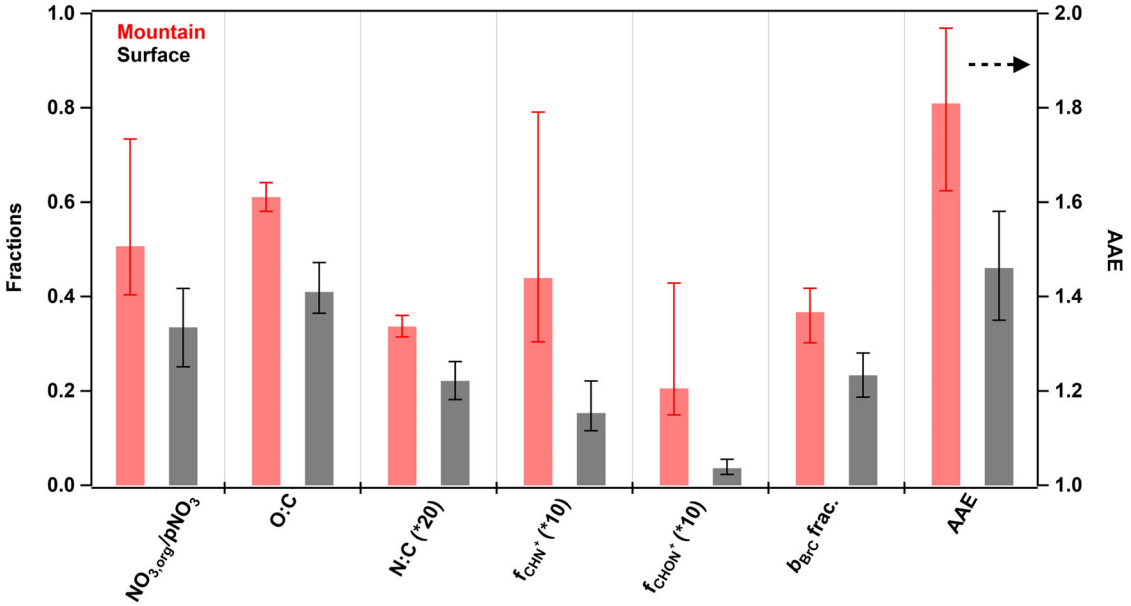

Fig. 5 | Comparison of the average contributions of several major substances or parameters at the mountain and surface sites. Fractions of particle-phase organic nitrates-to-total nitrate ($NO_{3,org}/pNO_3$), oxygen-to-carbon (O:C), nitrogen-to-carbon (N:C), CHN^+, $CHON^+$, fraction of brown carbon (BrC) absorption (b_{BrC}), and absorbing Ångström exponent (AAE, right *y* axis) for the mountain and surface site during the convective mixing period.

Methodology

Sampling site

We conducted field measurements at the surface site (Institute of Atmospheric Physics, Chinese Academy of Science; 39.97° N, 116.37° E; 50 m above sea level, a.s.l.) and the mountain site (Haituo Mountain; 40.52° N, 115.78° E, 1344 m a.s.l.) in Beijing, China. The mountain is located in the northwestern Beijing area. It is approximately 85 km north of the city center and was downwind of the central city throughout the sampling period, during which southerly winds prevailed. The ideal location of the mountain site is that it is located over the top of the PBL. Previous research has observed that surface-emitted pollutants mix with the convective boundary layer during the day and reach mountainous sites on a daily basis. Effective transport or formation of low-volatile substances from the ground to the top of the PBL was observed; however, semi-volatile substances decreased during the upward transport process[35].

The HR-AMS data were processed and analyzed using the standard AMS analysis. The AMS was calibrated for ionization efficiency using pure ammonium nitrate by following the standard protocols. Here, we apply two independent methods of quantifying pON. Note that the default relative ionization efficiencies of 1.1 and 1.4 were applied for inorganic nitrate and organic nitrate, respectively, during the mountain and surface campaigns. A constant collection efficiency of 0.5 was used for both experiments. The elemental composition of OA was calculated using the "improved-ambient" method. The relative ionization efficiency of the nitrogenous fragments CHN^+ and $CHON^+$ is 1.4. These are deemed as compositions of nitrogenous organic aerosols without interference of inorganic nitrate.

Quantification of organic nitrate

For most field applications of the AMS, aerosol nitrate concentrations are typically reported as a single inorganic nitrate concentration. This is due to the fact that nearly all of the signal is measured at a couple of common ion peaks (e.g., NO^+: *m*/*z* 30 and NO_2^+: *m*/*z* 46). However, a few reports showed that the *m*/*z* 46/30 ratio is substantially smaller than ammonium nitrate and suggested that these signals may be associated with organic nitrates[47]. The fraction of total AMS nitrate comprised of ON can be derived from the equation below (adapted from Eq. 1 in Farmer et al. [18], with modified notation for certain terms to align with this paper):

$$f_{NO3,org} = \frac{(R_{obs} - R_{NH_4NO_3})(1 + R_{NO3,org})}{(R_{NO3,org} - R_{NH_4NO_3})(1 + R_{obs})} \quad (1)$$

where $f_{NO3,org}$ is the fraction of organic nitrate in typical AMS nitrate; R_{obs}, R_{NH4NO3}, and $R_{NO3,org}$ denote the NO_2^+/NO^+ ratios for the observed ambient aerosol, pure NH_4NO_3, and $NO_{3,org}$, respectively. The pON/OA ratio investigated in this study pertains to the mass concentration of pON relative to the combined concentration of OA (Org plus $NO_{3,org}$). The molecular weight of pON is assumed to be 200 g mol^{-1} to convert $NO_{3,org}$ into pON[48]. Moreover, both R_{NH4NO3} and $R_{NO3,org}$ depend on the particular AMS. The ratio between both (χ) can be expressed as[49]:

$$\chi = \frac{R_{NH_4NO_3}}{R_{NO3,org}} \quad (2)$$

In the absence of pON standards, the pON NOx^+ ratio can be estimated using a ratio referenced to the calibrated ammonium nitrate ratio. So the value of $\chi = 2.75 \pm 0.41$ for urban environment[39] is used for this study.

The positive matrix factorization (PMF) method is also used to derive the organic nitrate (Supporting Information). Being different from the standard PMF method for organic mass spectra only, the mass spectral and error matrices of inorganic fragment ions are also integrated with those of OA into one unified dataset. The PMF analysis is performed on all the fragments of OA up to *m*/*z* 120, in particular also incorporating the nitrate fragments (NO^+ and NO_2^+) to assign these fragments with each resolved factor[19]. The nitrate fragment ions NO^+ (*m*/*z* 30) and NO_2^+ (*m*/*z* 46) before PMF analysis were also converted to mass concentrations in both data and error matrices. Each PMF resolved factor will contain NO^+ and NO_2^+ ions, and one factor with a significantly lower NO^+/NO_2^+ ratio compared to the others can be recognized as representing inorganic nitrate; whereas the other factors can be deemed as organic nitrate associated with certain sources determined by the OA mass spectra. The total concentration of organic nitrate can then be calculated by summing up the NO^+ and NO_2^+ mass from all OA factors. The NOx^+ ratio method produced similar results to conducting PMF on the expanded mass spectra series (including both OA and NOx^+ ions) to apportion nitrates.

The variation in light absorption coefficient (b_{abs}) as a function of wavelength (λ) is described by the absorbing Ångström exponent (AAE):

$$AAE = -\frac{\ln(b_{abs,\lambda_1}) - \ln(b_{abs,\lambda_2})}{\ln(\lambda_1) - \ln(\lambda_2)} \quad (3)$$

the λ_1 and λ_2 are selected at 370 nm and 880 nm, respectively. An AAE value of 1.0 is generally adopted for BC (black carbon). The differences in the AAE values were used to distinguish between BC and BrC[50].

The three-dimensional (3D) trajectories of air mass histories were computed using the Numerical Atmospheric-dispersion Modeling Environment[51], a Lagrangian dispersion model that employs Monte Carlo methods to track the 3D paths of plume parcels. The integrated time is recorded on a 0.25° × 0.25° horizontal grid, spanning from the ground up to 1000 meters in altitude, encompassing all particles for a given release period. To calculate the historical air mass contribution, the model releases tracer particles at a nominal rate of 1 g s^{-1}, with a maximum travel time of 24 hours in backward mode from the sampling site. The potential source contribution of particles to the mountain site over the past 24 hours is classified into four main regions (Supplementary Fig. 3): north (41.5° ~ 45° N, 104° ~ 121° E), south (32° ~ 39° N, 115° ~ 121° E) west (32° ~ 41.5° N, 104° ~ 115° E) and local (39° ~ 41.5° N, 115° ~ 117° E). The concentration of aerosols within these air masses is contingent upon factors such as transport efficiency, reaction rates, and deposition rates specific to each type of aerosol. The model differentiates between air masses that are influenced more locally and those that are influenced by regional transport from wider areas.

Data availability

The data that support the findings of this study are available from the authors on reasonable request.

Received: 18 March 2024; Accepted: 26 July 2024;
Published online: 04 August 2024

References

1. Rahman, K. M. A. & Zhang, D. Effects of fertilizer broadcasting on the excessive use of inorganic fertilizers and environmental sustainability. *Sustainability* **10**, 759 (2018).
2. Galloway, J. N. et al. Transformation of the nitrogen cycle: recent trends, questions, and potential solutions. *Science* **320**, 889–892 (2008).
3. Holland, E. A., Dentener, F. J., Braswell, B. H. & Sulzman, J. M. Contemporary and pre-industrial global reactive nitrogen budgets. *Biogeochemistry* **46**, 7–43 (1999).
4. Porter, E. M. et al. Interactive effects of anthropogenic nitrogen enrichment and climate change on terrestrial and aquatic biodiversity. *Biogeochemistry* **114**, 93–120 (2013).
5. Peñuelas, J. et al. Human-induced nitrogen–phosphorus imbalances alter natural and managed ecosystems across the globe. *Nat. Commun.* **4**, 2934 (2013).
6. Zare, A. et al. A comprehensive organic nitrate chemistry: insights into the lifetime of atmospheric organic nitrates. *Atmos. Chem. Phys.* **18**, 15419–15436 (2018).
7. Ng, N. L. et al. Nitrate radicals and biogenic volatile organic compounds: oxidation, mechanisms, and organic aerosol. *Atmos. Chem. Phys.* **17**, 2103–2162 (2017).
8. Horowitz, L. W. et al. Observational constraints on the chemistry of isoprene nitrates over the eastern United States. *J. Geophys. Res. Atmos.* **112**, D12S08 (2007).
9. Paulot, F., Henze, D. K. & Wennberg, P. O. Impact of the isoprene photochemical cascade on tropical ozone. *Atmos. Chem. Phys.* **12**, 1307–1325 (2012).
10. Travis, K. R. et al. Why do models overestimate surface ozone in the Southeast United States? *Atmos. Chem. Phys.* **16**, 13561–13577 (2016).
11. O'brien, J. M. et al. Measurements of alkyl and multifunctional organic nitrates at a rural site in Ontario. *J. Geophys. Res. Atmos.* **100**, 22795–22804 (1995).
12. Blando, J. D. et al. Secondary formation and the smoky mountain organic aerosol: an examination of aerosol polarity and functional group composition during SEAVS. *Environ. Sci. Technol.* **32**, 604–613 (1998).
13. Day, D. A. et al. A thermal dissociation laser-induced fluorescence instrument for in situ detection of NO_2, peroxy nitrates, alkyl nitrates, and HNO_3. *J. Geophys. Res. Atmos.* **107**, ACH 4-1–ACH 4-14 (2002).
14. Thieser, J. et al. A two-channel thermal dissociation cavity ring-down spectrometer for the detection of ambient NO_2, RO_2NO_2 and $RONO_2$. *Atmos. Meas. Tech.* **9**, 553–576 (2016).
15. Aruffo, E. et al. Partitioning of organonitrates in the production of secondary organic aerosols from α-pinene photo-oxidation. *Environ. Sci. Technol.* **56**, 5421–5429 (2022).
16. Fry, J. L. et al. Organic nitrate and secondary organic aerosol yield from NO_3 oxidation of β-pinene evaluated using a gas-phase kinetics/aerosol partitioning model. *Atmos. Chem. Phys.* **9**, 1431–1449 (2009).
17. Bruns, E. A. et al. Comparison of FTIR and particle mass spectrometry for the measurement of particulate organic nitrates. *Environ. Sci. Technol.* **44**, 1056–1061 (2010).
18. Farmer, D. K. et al. Response of an aerosol mass spectrometer to organonitrates and organosulfates and implications for atmospheric chemistry. *Proc. Natl Acad. Sci. USA* **107**, 6670–6675 (2010).
19. Sun, Y. L. et al. Factor analysis of combined organic and inorganic aerosol mass spectra from high resolution aerosol mass spectrometer measurements. *Atmos. Chem. Phys.* **12**, 8537–8551 (2012).
20. Yu, K., Zhu, Q., Du, K. & Huang, X. F. Characterization of nighttime formation of particulate organic nitrates based on high-resolution aerosol mass spectrometry in an urban atmosphere in China. *Atmos. Chem. Phys.* **19**, 5235–5249 (2019).
21. Xu, L. et al. Aerosol characterization over the southeastern United States using high-resolution aerosol mass spectrometry: spatial and seasonal variation of aerosol composition and sources with a focus on organic nitrates. *Atmos. Chem. Phys.* **15**, 7307–7336 (2015).
22. Xu, W. et al. Estimation of particulate organic nitrates from thermodenuder–aerosol mass spectrometer measurements in the North China Plain. *Atmos. Meas. Tech.* **14**, 3693–3705 (2021).
23. Nan, J. et al. Study on the daytime OH radical and implication for its relationship with fine particles over megacity of Shanghai, China. *Atmos. Environ.* **154**, 167–178 (2017).
24. Zang, H. et al. High atmospheric oxidation capacity drives wintertime nitrate pollution in the eastern Yangtze River Delta of China. *Atmos. Chem. Phys.* **22**, 4355–4374 (2022).
25. Morales, A. C. et al. The production and hydrolysis of organic nitrates from OH radical oxidation of β-ocimene. *Atmos. Chem. Phys.* **21**, 129–145 (2021).
26. Wennberg, P. O. et al. Gas-phase reactions of isoprene and its major oxidation products. *Chem. Rev.* **118**, 3337–3390 (2018).
27. Chen, J. et al. Particulate organic nitrates at Mount Tai in winter and spring: variation characteristics and effects of mountain-valley breezes and elevated emission sources. *Environ. Res.* **212**, 113182 (2022).
28. Horowitz, L. W., Liang, J., Gardner, G. M. & Jacob, D. J. Export of reactive nitrogen from North America during summertime: sensitivity to hydrocarbon chemistry. *J. Geophys. Res. Atmos.* **103**, 13451–13476 (1998).
29. Lee, B. H. et al. Highly functionalized organic nitrates in the southeast United States: contribution to secondary organic aerosol and reactive nitrogen budgets. *Proc. Natl Acad. Sci. USA* **113**, 1516–1521 (2016).
30. Perraud, V. et al. Nonequilibrium atmospheric secondary organic aerosol formation and growth. *Proc. Natl Acad. Sci. USA* **109**, 2836–2841 (2012).

31. Jiang, X. et al. Secondary organic aerosol formation from photooxidation of furan: effects of NO_X and humidity. *Atmos. Chem. Phys.* **19**, 13591–13609 (2019).
32. Laskin, A., Laskin, J. & Nizkorodov, S. A. Chemistry of atmospheric brown carbon. *Chem. Rev.* **115**, 4335–4382 (2015).
33. Cao, L. M. et al. Volatility measurement of atmospheric submicron aerosols in an urban atmosphere in southern China. *Atmos. Chem. Phys.* **18**, 1729–1743 (2018).
34. Paulson, S. S. & Orlando, J. J. The reactions of ozone with alkenes: an important source of HOx in the boundary layer. *Geophys. Res. Lett.* **23**, 3727–3730 (1996).
35. Liu, Q. et al. Reduced volatility of aerosols from surface emissions to the top of the planetary boundary layer. *Atmos. Chem. Phys.* **21**, 14749–14760 (2021).
36. Hu, W. W. et al. Insights on organic aerosol aging and the influence of coal combustion at a regional receptor site of central eastern China. *Atmos. Chem. Phys.* **13**, 10095–10112 (2013).
37. Zhao, J. et al. Organic aerosol processing during winter severe haze episodes in Beijing. *J. Geophys. Res.: Atmos.* **124**, 10248–10263 (2019).
38. Sun, Y. L. et al. Aerosol composition, sources and processes during wintertime in Beijing, China. *Atmos. Chem. Phys.* **13**, 4577–4592 (2013).
39. Day, D. A. et al. A systematic re-evaluation of methods for quantification of bulk particle-phase organic nitrates using real-time aerosol mass spectrometry. *Atmos. Meas. Tech.* **15**, 459–483 (2022).
40. Lin, C. et al. Primary and secondary organic nitrate in northwest china: a case study. *Environ. Sci. Technol. Lett.* **8**, 947–953 (2021).
41. Zhang, J. K. et al. Characterization of submicron particles during biomass burning and coal combustion periods in Beijing, China. *Sci. Total Environ.* **562**, 812–821 (2016).
42. Pullinen, I. et al. Impact of NO_X on secondary organic aerosol (SOA) formation from α-pinene and β-pinene photooxidation: the role of highly oxygenated organic nitrates. *Atmos. Chem. Phys.* **20**, 10125–10147 (2020).
43. Nishino, N., Atkinson, R. & Arey, J. Formation of nitro products from the gas-phase OH radical-initiated reactions of toluene, naphthalene, and biphenyl: effect of NO_2 concentration. *Environ. Sci. Technol.* **42**, 9203–9209 (2008).
44. Wang, Y. et al. The formation of nitro-aromatic compounds under high NO_X and anthropogenic VOC conditions in urban Beijing, China. *Atmos. Chem. Phys.* **19**, 7649–7665 (2019).
45. Fry, J. L. et al. Secondary organic aerosol (SOA) yields from NO3 radical + isoprene based on nighttime aircraft power plant plume transects. *Atmos. Chem. Phys.* **18**, 11663–11682 (2018).
46. Fan, M.-Y. et al. Important role of NO_3 radical to nitrate formation aloft in urban beijing: insights from triple oxygen isotopes measured at the tower. *Environ. Sci. Technol.* **56**, 6870–6879 (2022).
47. Marcolli, C. et al. Cluster analysis of the organic peaks in bulk mass spectra obtained during the 2002 new england air quality study with an aerodyne aerosol mass spectrometer. *Atmos. Chem. Phys.* **6**, 5649–5666 (2006).
48. Takeuchi, M. & Ng, N. L. Chemical composition and hydrolysis of organic nitrate aerosol formed from hydroxyl and nitrate radical oxidation of *α*-pinene and *β*-pinene. *Atmos. Chem. Phys.* **19**, 12749–12766 (2019).
49. Fry, J. L. et al. Observations of gas- and aerosol-phase organic nitrates at BEACHON-RoMBAS 2011. *Atmos. Chem. Phys.* **13**, 8585–8605 (2013).
50. Lack, D. A. & Langridge, J. M. On the attribution of black and brown carbon light absorption using the Ångström exponent. *Atmos. Chem. Phys.* **13**, 10535–10543 (2013).
51. Jones A., Thomson D., Hort M. & Devenish B. The U.K. Met Office's Next-Generation Atmospheric Dispersion Model, NAME III. *Air Pollution Modeling and Its Application XVII* (British Crown Copyright, Met Office, 2007).

Acknowledgements

This study was financially supported by the Zhejiang Province Science Fund for Distinguished Young Scholars (No. LR24D050001), National Natural Science Foundation of China (No. 42175116 and 42275121), Joint Funds of the Zhejiang Provincial Natural Science Foundation of China (Nos. LZJMZ23D050002) and Scientific Research Foundation for Guilin University of Technology (No. GUTQDJJ2023046). Part of this work was also supported by the Guangxi Engineering Research Center of Comprehensive Treatment for Agricultural Non-Point Source Pollution and the Modern Industry College of Ecology and Environmental Protection, Guilin University of Technology.

Author contributions

Y.W., D.L., and Q.L. designed the research; Y.W., D.L., P.T., X.J., K.H., S.L., F.W., M.H., and D.D. performed the research; Y.W., D.L., Q.L., P.T., and K.H. contributed analytic tools; Y.W., D.L., W.X., J.W., C.Y., and D.H. analyzed data; Y.W. and D.L. wrote the paper.

Competing interests

The authors declare no competing interests.

Additional information

Supplementary information The online version contains supplementary material available at https://doi.org/10.1038/s41612-024-00726-x.

Correspondence and requests for materials should be addressed to Dantong Liu.